Catalysis Science & Technology

Accepted Manuscript

ROYAL SOCIETY OF CHEMISTRY

www.rsc.org/catalysis

Catalysis Science & Technology

ARTICLE

Cobalt nanoparticles embedded in porous N-doped carbon as a long–life catalyst for hydrolysis of ammonia borane

Haixia Wang,[a] Yaran Zhao,[a] Fangyi Cheng,[a] Zhanliang Tao[a] and Jun Chen*[a,b]

Received 00th January 20xx,
Accepted 00th January 20xx

DOI: 10.1039/x0xx00000x

www.rsc.org/

Cobalt-based materials are promising catalysts for hydrolysis of ammonia borane. However, the stability of such catalysts is still a challenge for their application. We here report one-step synthesis of Co nanoparticles embedded in porous N-doped carbon (denoted as Co@N-C) and their enhanced catalytic stability for hydrolysis of ammonia borane. Co@N-C catalysts are fabricated through one-step thermolysis of Co(salen) at selected temperatures (600-800 °C) under Ar atmosphere. It is found that among the catalysts for this study, Co@N-C nanocomposite obtained at 700 °C (Co@N-C-700) shows superior catalytic activity and high sustainability. The turnover frequency (TOF) and activation energy of Co@N-C-700 for the hydrolysis of ammonia borane is 5.6 mol_{H2} mol_{Co}^{-1} min^{-1} and 31.0 kJ mol^{-1}, respectively. In particular, this catalyst retains 97.2% of its initial catalytic activity after 10 cycles. The remakable catalytic activity and durability of Co@N-C-700 are attributed to high dispersion of Co nanoparticles in porous N-doped carbon. This would provide insights into the enhancement of cycling utilization of Co@N-C-700 nanocomposite for catalytic hydolysis of ammonia borane.

1. Introduction

Ammonia borane (AB) has been considered as a desirable solid hydrogen carrier for portable hydrogen storage application due to its high hydrogen content (19.6 wt%).[1-3] Recently, hydrolysis of AB has been regarded as a popular and efficient approach because of its rapid hydrogen release and green process with catalysts.[4-7] Indeed, noble metal catalysts exhibited high catalytic activity.[8-10] However, high cost hindered their widespread applications.

It is essential to develop non-noble catalysts with high activity for hydrolysis of AB.[11-14] In the system of non-noble catalysts, Co displayed higher catalytic performance than that of Ni and Cu prepared under the same conditions[15-17] However, the agglomeration of Co nanoparticles (NPs) not only decreases its catalytic activity, but also makes its recycling performance very poor. To solve this problem, supporting materials such as hydroxyapatite, graphene, silica aerogel and macroscopic biopolymer hydrogel have been used for the dispersion of Co NPs.[18-24] For example, hydroxyapatite-supported cobalt catalyst was prepared by a two-step method including long-time (72h) ion exchange and the following reduction of Co^{2+}. The as-prepared catalyst with Co content of 0.72 wt% showed a high activation energy of 50 ± 2 kJ mol^{-1}, and 81% of the initial catalytic activity after 5 cycles.[18] Meantime, Co NPs were loaded on the surface of graphene, keeping 60% of the initial catalytic activity in the fifth cycle.[19] Thus, the durability and recycling ability of Co NPs are still to be improved.

Previous reports have shown that metal NPs such as Sn, Co, Fe, and Ni embedded in porous N-doped carbon exhibited excellent electrochemical performance in lithium-ion batteries and oxygen reduction.[25, 26] It is found that highly dispersed Co NPs can be synthesized through the direct thermal decomposition of M(salen = N,N'-bis(salicylidene)-ethylenediamin). To our knowledge, this kind of catalysts has not been applied to the hydrolysis of AB.

Herein, we report catalytic hydrolysis of AB in the presence of Co@N-C catalysts that were prepared by direct carbonization of Co(salen) at the temperature range of 600-800 °C under Ar atmosphere. Co NPs were homogenously distributed in porous N-doped carbon through this method. Co@N-C obtained at 700 °C showed a maximum hydrogen generation rate of 5.6 mol_{H2} mol_{Co}^{-1} min^{-1} and 97.2% of initial catalytic activity after 10 cycles. This highly catalytic performance and stability of Co@N-C-700 catalyst should offer light for the application in hydrolysis of AB.

2. Experimental section

2.1. Chemicals

N,N'-bis(salicylidene)-ethylenediamin (salen) and Co(salen) (97%) were purchased from J&K scientific LTD.

[a] Key Laboratory of Advanced Energy Materials Chemistry (Ministry of Education), Nankai University, Tianjin 300071, China
[b] Collaborative Innovation Center of Chemical Science and Engineering, Nankai University, Tianjin, 300071, China.
E-mail: chenabc@nankai.edu.cn; Fax: +86-22-23506808; Tel: +86-22-23506808
Electronic Supplementary Information (ESI) available: [Fig. S1-Fig.S2 and table S1-table S2]. See DOI: 10.1039/x0xx00000x

Ammonia borane (NH_3BH_3, 90%), cobalt chloride hexahydrate ($CoCl_2 \cdot 6H_2O$) and sodium borohydride ($NaBH_4$, 96%) were purchased from Sigma Aldrich. All the chemicals were put into use without further purification. Deionized water (DI water) was used in the whole process of experiments.

2.2 Synthesis of Co@N-C and Co/N-C catalysts

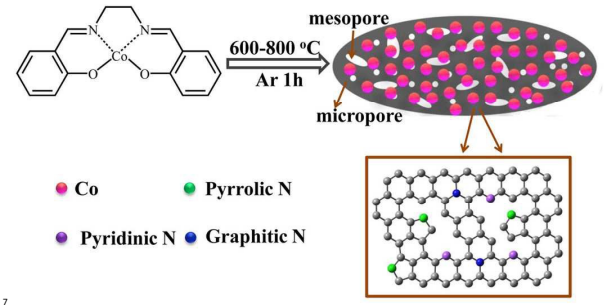

Fig. 1 Illustration for the forming process of Co@N-C catalysts prepared by pyrolysis of Co(salen) at selected temperatures of 600-800 °C under Ar atmosphere.

The fabrication procedure of Co@N-C composites is expressed in Fig. 1. Co@N-C catalysts were synthesized through a facile one-step method with the direct thermolysis of Co(salen) at temperatures of 600, 700 and 800 °C (denoted as Co@N-C-600, Co@N-C-700 and Co@N-C-800) under Ar for 1 h. Co^{2+} ions are bonded to N and O atoms of salen, leading to well distributed Co^{2+} in organic framework at molecular level. After calcination, Co NPs are uniformly introduced into porous N-doped carbon. For comparison, Co NPs were supported on the surface of porous N-doped carbon (denoted as Co/N-C) with the following steps. First, porous N-doped carbon was synthesized by the direct thermal decomposition of Co(salen) under Ar for 1 h. Second, 50 mg N-doped carbon was dispersed into 10 mL of deionized water under sonication for 30 min, followed by adding 10 mL of aqueous solution of $CoCl_2 \cdot 6H_2O$ (85 mg). The Co^{2+} was reduced to metal Co by adding 100 mg AB into the above solution. The whole experiment was carried out at 298 K. Finally, the mixed solution was filtrated and the obtained black powder was washed with deionized water and absolute ethanol, and dried in a vacuum oven at 60 °C for 10 h.

2.3 Catalytic hydrolysis of AB

Hydrogen generation rate of AB catalyzed by catalysts was measured at 298 K via a typical water displacement method. In general, 20 mg of Co@N-C-600, Co@N-C-700, Co@N-C-800 and Co/N-C catayst were placed into a one-neck round-bottom flask containing 8 mL of distilled water, and the mixture was stirred for a few minutes. Hydrogen began to produce when 40 mg of AB was added. The volume of hydrogen was calculated by the displacement of discharged water in an inverted burette. The hydrolysis reactions of AB were also performed at various temperatures ranging from 298 K to 328 K. The hydrolysis equation of AB is briefly presented as follows:

$$NH_3BH_3 + 2H_2O \rightarrow NH_4^+ + BO_2^- + 3H_2 \uparrow$$

2.4 The recycling test of Co@N-C-700 and Co/N-C

When the hydrolytic dehydrogenation of AB was completed, the catalysts were isolated by a permanent magnet. After a few minutes, the catalysts were magnetically attracted to the bottom of one-neck round-bottom flask. The supernatant liquid was removed. 40 mg of AB was added to the flask when the catalysts were washed with 8 mL deionized water. Such a recycle test was conducted for 10 runs under the same condition at 298 K.

2.6 Catalyst characterization

Power X-ray diffraction (XRD) was performed on a Rigaku Mini Flex 600 powder diffractometer (Cu Kα radiation, λ = 1.5406 Å). Raman spectra were obtained by a confocal Raman microscope (DXR, Thermo-Fisher Scientific). The content of Co was measured by inductively coupled plasma-atomic emission spectroscopy (ICP-AES, IRIS Advantage, Thermo). Elemental analysis was performed on a vario ELCUBE. X-ray photoelectron spectroscopic (XPS) measurements were carried out on a Versa Probe PHI 5000 system. The Brunauer–Emmett–Teller (BET) surface areas of the as-prepared samples were measured by nitrogen adsorption-desorption isotherms (BELSORP-Mini) at 77 K.

3. Results and discussion

Fig. 2a shows the XRD patterns of the as-prepared samples. A broad and weak peak around 26° can be indexed to (002) plane of carbon. The intensity of C (002) diffraction peak for Co@N-C-800 catalysts is higher, suggesting the greater degree of graphitization. In addition, the diffraction peaks located at 44.0°, 51.3° and 75.6° are consistent with JCPDS No.15-806, demonstrating the formation of Co NPs after the calcination of Co(salen) at 600-800 °C.

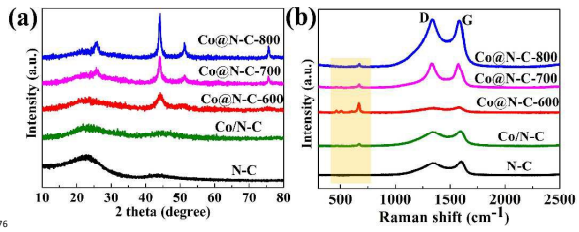

Fig. 2 (a) XRD patterns and (b) Raman spectra of N-doped carbon, Co/N-C, Co@N-C-600, Co@N-C-700 and Co@N-C-800.

Raman spectra were tested to further characterize the as-prepared samples. As shown in Fig. 2b, two broad peaks at 1338.0 and 1584.7 cm^{-1} are ascribed to D and G bands of carbon, respectively. Compared with N-doped carbon, three additional bands of Co-contained catalysts at 467, 509 and 673 cm^{-1} can be attributed to Co NPs.[27] Furthermore, the results of element analysis display that the content of carbon increases from 62.2 wt% to 69.57 wt%, while the content of nitrogen decreases from 5.04 wt% to 0.69 wt% with elevated temperature (Table S1). Co contents in Co@N-C-600, Co@N-C-700, Co@N-C-800 and Co/N-C catalysts determined by ICP-AES are 16.5, 19.7, 25.3 and 24.8 wt%, respectively (Table S2).

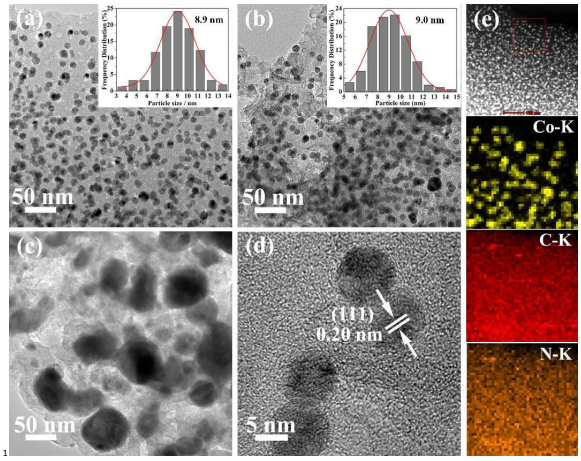

Fig. 3 TEM images of (a) Co@N-C-600, (b) Co@N-C-700 and (c) Co@N-C-800, (inset: size distributions of Co NPs), (d) HRTEM image and (e) elemental Co, C, and N mapping images of Co@N-C-700.

Fig. 3 shows the TEM images of Co@N-C composites prepared at different temperatures. As shown in Fig. 3a-b, when the pyrolysis of Co(salen) took place at 600 °C and 700 °C, Co NPs (black dots) with the size of about 9.0 nm (inset of Fig. 3a-b) are uniformly incorporated in porous N-doped carbon matrix (gray matrix). However, most of Co NPs begin to suffer from a serious aggregation when the temperature is increased to 800 °C. This implies that the temperature higher than 700 °C is not good for the dispersion of Co NPs (Fig. 3c). Fig. 3d displays the HRTEM image of Co@N-C-700, in which the d-spacing is measured to be 0.20 nm, which coincides with the (111) planes of Co NPs. Fig. 3e shows elemental Co, C and N mapping images of Co@N-C-700. N mapping shows that nitrogen is homogeneously doped into carbon matrix, which is consistent with the reported literature.[28] In order to investigate the effect of impregnation reduction and thermal reduction on the dispersion of Co NPs, Co/N-C (impregnation reduction) catalyst was prepared. Fig. S1 displays that Co NPs loaded on the surface of porous N-doped carbon are severely aggregated. This further demonstrates that thermal reduction is in favour of dispersing Co NPs.

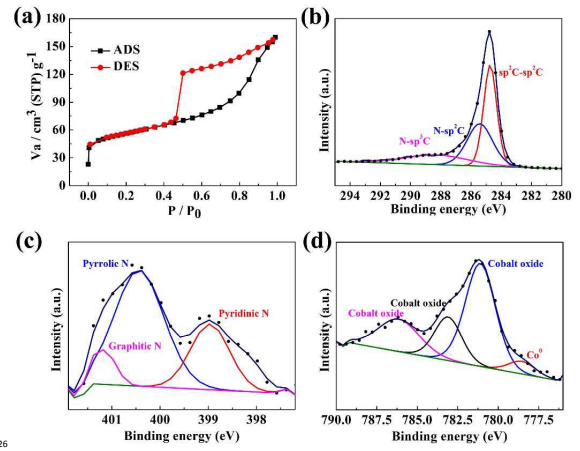

Fig. 4 (a) Nitrogen adsorption/desorption isotherm and high-resolution XPS spectra of (b) C1s, (c) N1s and (d) Co2p of Co@N-C-700.

The surface area of Co@N-C-700 catalyst was measured by nitrogen adsorption/desorption isotherm. As shown in Fig. 4a, the adsorption/desorption isotherm can be defined as type IV according to the IUPAC nomenclature.[29] On the basis of Horvath-Kawazoe (HK) method, the pore size distribution of micropore is focused on 0.78 and 1.31 nm (Fig. S2a). The mesopore size distribution is centralized at 5.29 nm (Fig. S2b) based on Barrett-Joyner-Halenda (BJH) model. The determined BET specific surface area of Co@N-C-700 is 182.3 m^2 g^{-1}. A large surface area and plenty of micropores and mesopores could make a significant contribution to the full infiltration of AB aqueous solution. The surface of Co@N-C-700 was further studied by XPS (Fig. 4b). Three peaks of C1s spectrum can be observed at 284.8, 285.5, and 288.7 eV, respectively. This indicates the presence of C=C, C=N and C-N, respectively.[30] The high-resolution spectrum of N1s reveals three peaks with binding energy of 398.9, 400.4, and 401.2 eV (Fig.4c), which are corresponded to pyridinic N, pyrrolic N and graphitic N, respectively.[31] The high-resolution spectrum of Co2p was depicted in Fig. 4d. The peak at around 778.6 eV is in accordance with binding energy of zero-valent Co, confirming that Co NPs can be successfully synthesized by thermal reduction of Co(salen) at high temperature. The peaks at 781.1, 783.1 and 787.7 eV are ascribed to cobalt oxide,[30, 32] which may be formed during the XPS sampling.

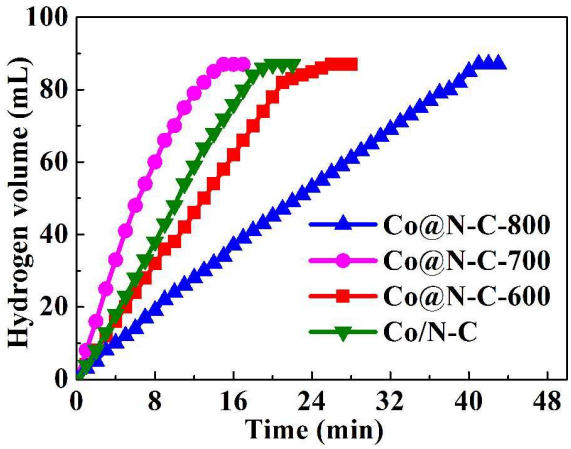

Fig. 5 Hydrogen generation from the hydrolysis of AB catalyzed by C/N-C, Co@N-C-600,Co@N-C-700 and Co@N-C-800 catalysts at 298 K.

The unique morphology and structure of the as-synthesized Co@N-C catalysts inspire us to study their catalytic performances for the hydrolysis of AB. All the catalytic hydrolysis reactions of AB were carried out at 298 K. Fig. 5 shows that the volume of released hydrogen is about 87 mL, indicating the hydrolysis reaction of AB is almost completed. Hydrogen generation rate of AB catalyzed by Co/N-C, Co@N-C-600, Co@N-C-700 and Co@N-C-800 are 2.14, 2.88, 5.6 and 1.16 mol_{H2} mol_{Co}^{-1} min^{-1}. Among them, Co@N-C-700 exhibits the highest catalytic performance attributing to highly

dispersed Co NPs. Furthermore, compared with that of Co based catalysts in Table 1, Co@N-C-700 catalyst also exhibits a relatively high catalytic activity. The poorly catalytic performances of Co@N-C-800 and Co/N-C catalysts are attributed to the loss of active sites owing to the agglomeration of Co NPs. These results show that the preparation of Co@N-C catalysts is easier, and the high dispersion and small size of Co NPs are also beneficial for improving catalytic performance of Co catalysts.

The effect of temperature on hydrogen generation rate of AB was investigated by varying temperature from 298 K to 328 K. Fig. 6a shows hydrogen evolution rate at selected temperatures. The hydrogen evolution rate increases when the temperature is increased. This suggests that high temperature is conducive to improve the hydrogen generation rate of AB. The rate constant *k* at various temperatures (T) can be obtained according to the slope of fitting line and the ideal gas state equation. Activation energy (Ea) is calculated according to the following Arrhenius equation: [33]

$$\ln k = \ln A - Ea/RT$$

Fig. 6b shows Arrhenius plot of ln *k* versus 1000/T (Ea/R). The activation energy is calculated to be 31.0 kJ mol^{-1}. In comparison with most reported Co-based catalysts in Table 1, Co@N-C-700 catalyst shows a lower activation energy.

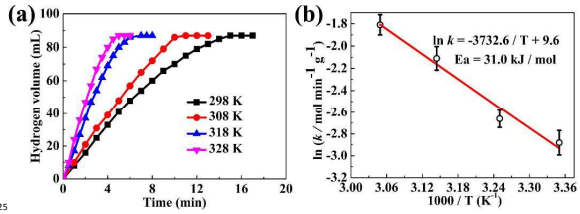

Fig. 6 (a) Hydrogen generation rate influenced by temperature in the presence of Co@N-C-700 catalyst and (b) the corresponding Arrhenius plot of ln *k vs* 1000/T

Table 1 Comparison of various Co-based catalysts for hydrolysis of AB.

Catalysts	TOF (mol_{H2} mol_{cat}^{-1} min^{-1})	Ea (kJ mol^{-1})	Recycles	Stability	Ref.
Co/graphene	13.8	32.75	5th	60%	19
PSMA-Co	25.7	34 ± 1	-	-	34
Co	0.88	-	-	-	35
10 wt% Co/γ-Al_2O_3	2.08	62	-	-	36
Amine-capped Co	39.9	28.2	5th	65.6%	37
p(VPA)-Co	7.67 (303 K)	25.51	-	-	38
Co/SAG	7.17	46.4	-	-	20
AuCo alloy	6.0	-	-	-	39
Co/hydroxyapatite	4.54	50 ± 2	5th	81%	18
Silica embedded cobalt(0)	-	42± 2	5th	74%	40
Co derived from MOF	-	35.5	-	-	41
intrazeolite cobalt(0) nanoclusters	5.32	56± 2	5th	69%	42
Co thin film	-	59 ± 1	6th	60%	43
Ti supported Co film	1.7	28.0	-	-	44
Co@N-C-700	5.6	31.0	10th	97.2%	This study

The durability and stability of catalysts play a key role in practical application. The recycling stability of Co/N-C and Co@N-C-700 catalysts was measured by adding additional AB (40 mg) with the catalysts isolated from the reaction solution. As shown in Fig. 7a, the hydrolytic rate of AB catalyzed by Co/N-C catalyst decreases sharply and only 38.6% of original catalytic activity is preserved in the 5th cycle, while Co@N-C-700 catalyst shows a good stability with 98.2% of initial catalytic activity after 5 cycles, 97.2% in the 10th cycle. These results indicate that Co@N-C-700 has a better stability than that of Co NPs supported on the surface of N-doped carbon. In comparison with Co based catalysts reported (Table 1), Co@N-C-700 catalyst also reveals the highest durability. Fig. 7b shows XRD patterns of Co@N-C-700 before and after 10 cycles, in which the diffraction peaks of metal Co become weaker after 10 cycles. The Co@N-C-700 catalyst may be activated by AB during the hydrolysis reaction. The microstructure of Co@N-C-700 after 10 cycles was characterized by TEM (Fig. 7c and d). Co NPs can still maintain original dispersion after 10 cycles. This further demonstrates that Co@N-C-700 nanocomposite is a long-lived catalyst for catalytic hydrolysis of AB.

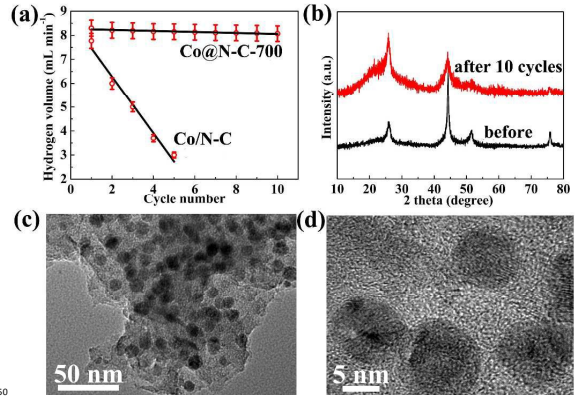

Fig. 7 (a) The recycling stability of Co/N-C and Co@N-C-700catalysts for the hydrolysis of AB during cycle numbers, (b) XRD patterns before and after 10 cycles, (c) TEM image and (d) HRTEM image of Co@N-C-700 after 10 cycles.

Conclusions

In summary, Co NPs embedded in porous N-doped carbon, which were synthesized by carbonization of Co(salen) at the temperature range of 600-800 °C under Ar atmosphere, have shown enhanced durability for catalytic hydrolysis of ammonia borane. Co NPs encapsulated in porous N-doped carbon have also shown well-defined micropores and mesopores. The hydrolysis rate of AB catalyzed by the catalyst prepared at 700 °C can attain 5.6 mol_{H2} mol_{Co}^{-1} min^{-1} with the activation energy of 31.0 kJ mol^{-1}. Furthermore, such catalyst can still retain 97.2% of initial catalytic activity even after 10 cycles. This means that Co NPs embedded in porous N-doped carbon is potential for the application in catalytic hydrolysis of ammonia borane.

Acknowledgements

This work was supported by National NSFC (51371100 and 51271094), and Tianjin High-Tech (13SJCZDJC26500 and 12JCQNJC03900).

Notes and references

1 B. Peng and J. Chen, *Energy Environ. Sci*., 2008, **1**, 479.
2 Y. Cheng, Y. Q. Fan, Y. Pei and M. H. Qiao, *Catal. Sci. Technol.*, 2015, **5**, 3903-3916.
3 J. Du, F. Cheng, M. Si, J. Liang, Z. Tao and J. Chen, *Int. J. Hydrogen Energy*, 2013, **38**, 5768.
4 U. B. Demirci and P. Miele, *Phys. Chem. Chem. Phys.*, 2014, **16**, 6872.
5 H. Wang, L. Zhou, M. Han, Z. Tao, F. Cheng and J. Chen, *J. Alloys Compd.*, 2015, **651**, 382.
6 X. Shan, J. Du, F. Cheng, J. Liang, Z. Tao and J. Chen, *Int. J. Hydrogen Energy*, 2014, **39**, 6987.
7 F. Cheng, H. Ma, Y. Li and J. Chen, *Inorg. Chem.*, 2007, **46,** 788.
8 W. Y. Chen, J. Ji, X. Feng, X. Z. Duan, G. Qian, P. Li, X. G. Zhou, D. Chen and W. K. Yuan, *J. Am. Chem. Soc.*, 2014, **136**, 16736.
9 H. Y. Ma and C. Z. Na, *ACS Catal.*, 2015, **5,** 1726.
10 X. Yang, F. Cheng, J. Liang, Z. Tao and J. Chen, *Int. J. Hydrogen Energy*, 2009, **34**, 8785.
11 L. Zhou, T. Zhang, Z. Tao and J. Chen, *Nano Res.*, 2014, **7**, 774.
12 J. Li, Q.-L. Zhu and Q. Xu, *Catal. Sci. Technol.*, 2014, **5**, 525.
13 J. Yang, F. Cheng, J. Liang and J. Chen, *Int. J. Hydrogen Energy*, 2011, 36, 1411-1417.
14 Y. C. Luo, Y. H. Liu, Y. Hung, X. Y. Liu and C. Y. Mou, *Int. J. Hydrogen Energy*, 2013, **38**, 7280.
15 S. Yildiz, N. Aktas and N. Sahiner, *Int. J. Hydrogen Energy*, 2014, **39**, 14690.
16 N. Sahiner and S. Yildiz, *Fuel Process. Technol.*, 2014, **126**, 324.
17 N. Sahiner and S. Sagbas, *J. Power Sources*, 2014, **246**, 55.
18 M. Rakap and S. Özkar, *Catal. Today*, 2012, **183**, 17.
19 L. Yang, N. Cao, C. Du, H. Dai, K. Hu, W. Luo and G. Cheng, *Mater. Lett.*, 2014, **115**, 113.
20 P. J. Yu, M. H. Lee, H. M. Hsu, H. M. Tsai and W. C. Y. Yui, *RSC Adv.*, 2015, **5**, 13985.
21 L. Ai, X. Gao and J. Jiang, *J. Power Sources*, 2014, **257**, 213.
22 T. Umegaki, J. M. Yan, X. B. Zhang, H. Shioyama, N. Kuriyama and Q. Xu, *J. Power Sources*, 2010, **195**, 8209.
23 Q. Xu and M. Chandra, *J. Power Sources*, 2006, **163**, 364.
24 Ö. Metin and S. Ö zkar, *Energy Fuels*, 2009, **23**, 3517.
25 Z. Zhu, S. Wang, J. Du, Q. Jin, T. Zhang, F. Cheng and J. Chen, *Nano Lett.*, 2014, **14**, 153.
26 J. Du, F. Cheng, S. Wang, T. Zhang and J. Chen, *Sci. Rep.*, 2014, **4**, 4386.
27 M. Galaburda, V. Bogatyrov, O. Oranska, V. Gun'ko, J. Skubiszewska-Zięba and I. Urubkov, *J. Therm. Anal. Calorim.*, 2015, **122**, 553.
28 X. Wang, W. Zhong and Y. Li, *Catal. Sci. Technol.*, 2015, **5**, 1014.
29 M. Kruk and M. Jaroniec, *Chem. Mater.*, 2001, **13**, 3169.
30 Y. Su, Y. Zhu, H. Jiang, J. Shen, X. Yang, W. Zou, J. Chen and C. Li, *Nanoscale*, 2014, **6**, 15080.
31 Z. Liu, L. Ji, X. Dong, Z. Li, L. Fu and Q. Wang, *RSC Adv.*, 2015, **5**, 6259.
32 S. Chao, Z. Bai, Q. Cui, H. Yan, K. Wang and L. Yang, *Carbon*, 2015, **82**, 77.
33 I. Matsumoto, K. Asano, K. Sakaki and Y. Nakamura, *Int. J. Hydrogen Energy*, 2011, **36**, 14488.
34 Ö. Metin and S. Özkar, *Int. J. Hydrogen Energy*, 2011, **36**, 1424.
35 X. Yang, F. Cheng, Z. Tao and J. Chen, *J. Power Sources*, 2011, **196**, 2785.
36 Q. Xu and M. Chandra, *J. Power Sources*, 2006, **163**, 364.
37 J. Hu, Z. Chen, M. Li, X. Zhou and H. Lu, *ACS Appl. Mater. Inter.*, 2014, **6**, 13191.
38 N. Sahiner and L. Sagbas, *J. Power Sources*, 2014, **246**, 55.
39 J. M. Yan, X. B. Zhang, T. Akita, M. Haruta and Q. Xu, *J. Am. Chem. Soc.*, 2010, **132**, 5326.
40 Ö. Metin, M. Dinc, Z. S. Eren and S. Özkar, *Int. J. Hydrogen Energy*, 2011, **36**, 11528.
41 P. Song, Y. Li, W. Li, B. He, J. Yang and X. Li, *Int. J. Hydrogen Energy*, 2011, **36**, 10468.
42 M. Rakap and S. Ozkar, *Int. J. Hydrogen Energy*, 2010, **35**, 3341.
43 M. Paladini, G. M. Arzac, V. Godinho, M. C. J. D. Haro and A. Fernández, *Appl. Catal. B-Environ.*, 2014, **158–159**, 400.
44 J. Liao, H. Li and X. Zhang, *Catal. Commun.*, 2015, **67**, 1.